Multireflection Effect on Formation of Periodic Surface Structure on an Si Film Melting-Crystallized by a Linearly Polarized Nd:YAG Pulse Laser Beam

Susumu Horita*, Hirokazu Kaki†, and Kensuke Nishioka

Japan Advanced Institute of Science and Technology, 1-1 Asahidai, Nomi, Ishikawa 923-1292, Japan

Abstract

We investigated the multireflection effect on the formation of a periodic surface structure produced by a linearly polarized Nd:YAG laser beam of 532 nm on an Si film deposited on a glass substrate, as well as on heating rate in the film, compared with an excimer laser beam. From the theoretical calculation results, it was found that the formation of the periodic surface structure and heating rate strongly depended on film thickness or that they were influenced by the multireflection effect. The thickness most effective for forming the periodic surface structure and heating rate was about 60 nm. Furthermore, we attempted to verify the calculation results by carrying out an experiment in which we checked whether the periodic structure was formed on the surface of the melting-crystallized Si films. As a result, the thickness range for producing the periodic surface structure was found to be from 50 to 70 nm, which were larger than the theoretical values of 40 to 60 nm.

KEYWORDS: multireflection, Si film, crystallization, green laser, YAG laser, TFT

* E-mail address: horita@jaist.ac.jp

† Present address: Process Research Center, Nissin Electric Co., Ltd., 47 Umezu-Takase-cho, Ukyo-ku, Kyoto 615-8686, Japan.

1. Introduction

Low-temperature polycrystalline silicon (LT poly-Si) thin film transistors (TFTs) are widely used for various applications. Among many methods of fabricating LT poly-Si films, a pulse laser annealing (PLA) method, in which an Si film deposited on an inexpensive glass substrate is melted by pulse laser irradiation so that it can be crystallized in a very short time, is effective for producing crystallized Si films with larger grain with high carrier mobility.[1,2] However, ideal TFTs require active regions entirely free of grain boundaries which reduce carrier mobility, cause the fluctuation of threshold voltage, and increase the off-current of transistors. In order to suppress the generation of grain boundaries, it is necessary to control temperature distribution in an irradiated Si film so as to reduce random nucleation and unify the solidification direction of molten Si. For this requirement, some researchers have proposed modulated PLA methods using absorption layer,[3,4] pre-patterned Si layer[5] and so on.[6-9] Interference PLA methods using a beamsplitter [10] or a phase-shift mask[11,12] have also been developed.

We have reported that, using a spatially periodic distribution of beam energy density (periodic E-D) induced spontaneously by irradiation with a linearly polarized laser beam, we can control the location of grain boundaries in an Si film crystallized on a Pyrex glass substrate.[13,14] The advantage of this method over the above-mentioned conventional methods is non-requirement for additional fabrication processes or optical components. That is, it is a very simple annealing process requiring only laser irradiation to control the temperature profile in a molten Si film. In this method, we used a Nd:YAG pulse laser with a wavelength λ of 532 nm. The generated periodic E-D has one-dimensional function like $\cos(x)$ on the irradiated surface of the Si film (x-y plane).[15-20] The maximum energy density lines or the minimum ones are parallel to one another along the y direction with a regular periodic distance of near λ (normal incident case) and are perpendicular to the electric field vector $\boldsymbol{E}$ of the incident beam. The periodic E-D produces the spatially periodic distribution of temperature (periodic T-D) in the irradiated Si film, in which the periodic T-D becomes similar to the periodic E-D. At each line region of the minimum temperature in the periodic T-D, nucleation of Si occurs and solidification extends almost perpendicularly to both the

nearest neighboring high-temperature regions. Then, the two adjoining solidification fronts which proceed toward each other in opposite directions collide at the periodic line region of the maximum temperature. So, grain boundaries are generated along the periodic collision line perpendicular to $\boldsymbol{E}$ or parallel to the y direction. As a result, over the whole melting-crystallized Si film, the location of grain boundary generation is controlled to be periodically perpendicular to $\boldsymbol{E}$ with the spatial period $\Lambda \approx \lambda$ at normal incidence. The periodic grain boundary accompanies the periodic structure on the surface of the crystallized Si film because the line regions of the periodic grain boundary are higher or hills due to the collision of the solidification fronts in the molten Si film.[21, 22)]

Generally, for melting-crystallization of an Si film, an excimer laser beam is mainly used at the wavelength of 308 or 254 nm. This is because the absorption length in Si, e.g. , 6.76 nm for 308 nm is much smaller than the Si film thickness of TFT < 100 nm, which generates the Si film heat much effectively, compared with a green laser beam whose absorption length in Si for 532 nm is about 1100 nm at room temperature.[23)] However, as mentioned above, we and other researchers[10, 24-26)] have already performed the melting-crystallization of Si films using green laser beams. Although a green laser beam travels in an Si film, it is multireflected in the film between the incident atmosphere and the glass substrate, so that it can be multiabsorbed. This effect possibly reduces the threshold laser beam energy or minimum energy for melting the Si film. Therefore, the threshold laser beam energy should be determined from not only absorption length but also the multireflection effect. Furthermore, in our case, because the origin of the periodic E-D generation is interference between the primary coherent incident beam and the high-order diffracted beams on the irradiated surface, the phase matching among the primary incident beam and multireflected beams at the surface of the Si film is a very important factor for periodic E-D generation. This means that the degree of E-D generation or the formation of the periodic surface structure strongly depends on the thickness of the Si film where multireflection occurs.[27)]

Thus, first, we investigated theoretically the multireflection effect on the heating of an Si film using a green laser beam of 532 nm, compared with an excimer laser beam of 308 nm. Second, the periodic E-D for 532 nm was calculated theoretically, taking the multireflection effect into account,

and the theoretical calculations were verified experimentally. In this paper, we show the calculation results of the multireflection effect on the heating of an Si film and the generation of periodic E-D. Next, we show the experimental results to determine whether the periodic surface structure of grain boundary is formed in an Si film deposited on a glass substrate, where the film thickness is varied from 46 to 78 nm. If the primary incident beam and the diffracted beams are out of phase from each other, the periodic surface structure, as well as the periodic E-D, fails to form. Finally, we discuss the differences between the theoretical and experimental results.

2. Theoretical

First, we consider the multireflection effect on the heating of an Si film by irradiation with a YAG laser (532 nm), as compared with irradiation with an excimer laser (308 nm). In order to take into account the multireflection in the Si film between the interfaces of vacuum/Si and Si/substrate for 532 nm, we used a model shown in Fig. 1. $\boldsymbol{E}_{\mathrm{i}}$ is the electric field of the primary incident laser beam, $\boldsymbol{E}_{\mathrm{r}}$ is the sum of the multireflected electric fields from the surface of the Si film and $\boldsymbol{E}_{\mathrm{t}}$ is the sum of the multitransmitted electric fields through the Si film to the glass substrate. R_{m} and r_{m} are the overall power reflectance and the overall amplitude reflectivity coefficient, respectively, from the surface of the Si film, and T_{m} is the overall power transmittance through the Si film. R_{m}, r_{m} and T_{m} are dependent on the Si film thickness d. θ_{i} is the incident angle, and ψ_1 and ψ_2 are the refractive angles in the medium of Si and SiO_2, respectively. n_{a} is the refractive index of the incident atmosphere, being almost equal to the vacuum index n_0. We calculated heating rate, i.e., the time-dependent temperature of the surface from the beginning of pulse irradiation as an indication of the heating effect, using the two-dimensional finite difference heat transport equation.[22,28)] In this calculation, the heat source term $S(T(t), z)$is expressed as

$$S(d,T(t),z) = [1 - R_m(d,T(t))]P(t)\alpha(T(t))\exp[\alpha(T(t))z], \qquad (1)$$

where t is the time, T is the temperature, R_{m} is film-thickness- and temperature-dependent overall power reflectance, P is the time-dependent laser beam energy density, and α is the temperature-dependent absorption coefficient. z is the vertical distance from the surface of the Si

film to the substrate, i.e., negative direction. For the excimer laser with 308 nm, it was assumed that the α was temperature-dependent as 1.43×10^{6}exp(T/4700) 1/cm [29] although the R_m was independent of d and a constant of 0.587 at room temperature because of the short absorption length and the slight dependence on temperature. On the other hand, for a YAG laser of 532 nm, both the R_m and α were temperature-dependent. The R_m was calculated from the complex refractive index as $4.153+5\times10^{-4}(T\text{-}300)-i0.038\exp[(T\text{-}300)/430)]$ and the α was 5.02×10^{3}exp(T/430) 1/cm.[29] According to this temperature-dependent α, the calculated absorption length decreases from ~1100 to 40 nm with increasing temperature. Although, strictly, the energy absorption in the Si film for 532 nm is not distributed exponentially as in the case of eq. (1) due to the multireflection in the film, we adopted this assumption for simplicity of calculation. This is not a very serious problem not only because the multireflection effect is included in the calculation of R_m but also because the thermal diffusion length, e.g., > 100 nm for 1 ns, is larger than a typical film thickness used in TFTs, i.e., 50 nm. Furthermore, it is assumed that the time-dependence of the beam energy profile is expressed by a Gaussian-like function with a full width at half maximum (FWHM) of 25 ns for each laser and the total irradiation time of 50 ns. In order to clarify the difference in heating effect between the two lasers, the calculation conditions except wavelength are provided to be same and we calculated the surface temperature of the Si film on the SiO_2 substrate from room temperature to the melting point of Si.

Next, we consider the multireflection effect in the theoretical calculation of the periodic E-D generated on the solid and molten Si films, for which we assumed that their optical properties are independent of temperature to simplify the calculation, i.e., at room temperature or melting point. This assumption is not perfect for accurate estimation, in particular, of solid films, but sufficient for understanding the physical essential behavior in periodic E-D generation. Although the initial surface of an as-deposited solid film has no periodic but almost random surface roughness with very small height, the surface roughness is composed of surface gratings with many various spatial periods. Therefore, it may have a special periodic component to produce a diffracted beam traveling on the surface. The intensity of this traveling beam is modified owing to the interaction of waves

between the primary incident beam and the diffracted beams. This modification depends on surface roughness with the special periodic component and it produces a periodic E-D. If the surface roughness of the special component is slightly increased due to faint amplitude of the periodic E-D at the first pulse irradiation, the increased surface roughness leads to increase in diffracted beam intensity, which increases modulation in the E-D at the next irradiation. Thus, the modifications of the surface roughness and the E-D enhance each other with a positive feedback loop.[18)]

Our analysis is based on Guosheng's theoretical report of the periodic E-D generated on the periodically corrugated surface of a sample.[30)] Because Guosheng's model is available only for the surface of opaque materials such as opaque molten Si films, not for transparent thin films in which multireflection occurs as shown in Fig. 1, we developed a modified analysis model of periodic E-D for a thin film deposited on a transparent substrate before.[31)] The analysis of Guosheng's model is performed just on the surface of a bulk medium, and the formula of periodic E-D is dependent on the refractive indexes of the incident atmosphere and irradiated medium. Hence, we introduced the effective refractive index N or an optically equivalent refractive index for the primary incident beam at the irradiated surface. Using this N, we can treat a thin film sample as a bulk medium effectively in the calculation of the periodic E-D. For normal incidence considered in this study, N can be expressed with r_m for an Si film with the thickness of d as

$$N(d) = n_0 \frac{1 - r_m}{1 + r_m}, \qquad (2)$$

where N is a function of d. This equation is easily obtained from the bulk standard formula in optics by substituting r_m and N instead of bulk reflectivity coefficient and bulk refractive index, respectively, in it. In the calculation of r_m, we used the Si complex refractive index n_{Si} of 4.153+i0.038 in solid phase. Diffraction of the primary incident laser beam occurs on a sinusoidally corrugated surface of the film as illustrated in Fig. 2(a). The corrugated vacuum-solid interface is described by $z(x)=-h\cdot\cos(2\pi x/\Lambda)$, where h is the amplitude of the corrugation, the z axis is outward normal to the macroscopic surface and the x axis is perpendicular to the periodic hill or ridge. Using the effective refractive index $N(d)$, we show the model for calculation in Fig. 2(b). The nth-order

reflected and refracted waves are generated owing to diffraction of the incident beam at the incident angle θ_i.

The Poynting vector modulated by the diffraction can be calculated on the basis of the standard diffraction theory and using Maxwell's equations, and the normal component of the time-average Poynting vector, $P_n(x)$, just inside the medium can be expressed approximately as

$$P_n(x) \cong P_0\left[1 + A\cos\left(\frac{2\pi}{\Lambda}x - \phi_p\right)\right] = P_0\left[1 + P_c\cos\left(\frac{2\pi}{\Lambda}x\right) + P_s\sin\left(\frac{2\pi}{\Lambda}x\right)\right], \quad (3)$$

where $P_0 > 0$ is a dc or average component, $A > 0$ is an ac amplitude ratio, and ϕ_p is the phase difference between the sinusoidal surface corrugation and $P_n(x)$. Moreover, $P_c \equiv A\cos\phi_p$ and $P_s \equiv -A\sin\phi_p$. The ac term comes from the interaction between waves of the zeroth order and the first order, and is proportional to h. The details are mentioned in ref. 26. Hereafter, we use this P_n as a formula of the periodic E-D. In the case of normal incidence $\theta_i = 0$, ϕ_p becomes 0 or ±180°. The physical meaning of $\phi_p = \pm 180°$ or $P_c < 0$ is to that the beam energy is absorbed more in the "hills" than in the "valleys" of the corrugation whereas that of $\phi_p = 0$ or $P_c > 0$ means to just the opposite situation. At $\phi_p = \pm 180°$, because the hills or ridge regions are heated more than the valley regions, and the higher temperature molten regions are cooled later, the height of the corrugation increases after solidification. Thus, owing to this increased h, A in $P_n(x)$ at the next irradiation is enhanced so that a clearer periodic E-D can be generated. Hence, the condition of $\phi_p = \pm 180°$ or $P_c < 0$ brings a positive feedback loop for the formation of the periodic surface structure of the grain boundary. In contrast, when $\phi_p = 0$ or $P_c > 0$, the valley regions are more heated and the irradiated Si film surface becomes flattened. Then, A in $P_n(x)$ decreases and the periodic E-D vanishes. Therefore, this condition is unfavorable for the formation of the periodic surface structure.

For the calculation of r_m, we assumed that the surface is not corrugated sinusoidally as shown in Fig. 2 but flat as shown in Fig. 1 for simplicity. According to eq. (2), because N is independent of corrugated surface roughness and is average over the surface, it neither contains the multireflection effect accurately nor corresponds to the actual rough surface. However, this calculation may provide give us essential information on the multireflection effect on the periodic E-D or the periodic

surface structure of the grain boundary. Because a typical h used in the calculation was 1 nm and much smaller than a Si film thickness of ≥ 30 nm used in this study, the inaccuracy is small. A 1-nm-height h is large enough for the purpose of estimating the multireflection effect because the actual generation of the periodic E-D is a positive feedback process so that the amplitude of $P_n(x)$ can be enhanced automatically.

3. Experimental

An amorphous silicon (a-Si) film with a thickness of 46 to 78 nm was deposited on a Pyrex glass at 350°C in an ultrahigh vacuum chamber. Then, the Si film was transferred in another chamber and was irradiated with a linearly polarized Nd:YAG pulse laser (wavelength: 532 nm, repetition frequency: 10 Hz, pulse width: 6-7 ns) at room temperature in another vacuum chamber. The other laser irradiation conditions were as follows: The laser energy density F was from 110 to 170 mJ/cm^2, the irradiation pulse number N_p was 2, and the beam incident angle θ_i was 0. The formation of the periodic surface structure on the crystallized Si film was examined by Nomarski optical microscope observation of its surface. The observation of the periodic surface structure indicates the generation of the periodic E-D on the film surface.[22, 32)]

4. Results and Discussion

First, we show the multireflection effect on heating of the irradiated film by theoretical calculation and discuss it. Figure 3 shows the theoretical calculation results regarding the dependences of the absorptivity A_m and the absorptivity per unit thickness a_m on the film thickness d for 532 nm. A_m and a_m are defined as $1-R_m-T_m$ and A_m/d, respectively. a_m indicates how the whole film is heated effectively because it corresponds to heat source density per unit thickness due to the beam energy penetrating into the film. We can see clearly from this figure how the multireflection effect influences the optical absorption of the Si film for 532 nm. A_m and a_m depend strongly on d and each has a maximum between 60 and 70 nm. From this result, it can be said that about 60 nm is the most effective thickness to heat and melt the film thicker than 15 nm. When the thickness is less

than 15 nm, the molten film is separated and eventually the solid Si islands are distributed on the glass substrate owing to the low wettability to SiO_2.[31)]

Figure 4 shows the time-dependences of surface temperature of an irradiated Si film on a SiO_2 substrate for 308 nm (excimer) and 532 nm(Nd:YAG) for the film thicknesses of 40, 60 and 80 nm. For both wavelengths, F is 250 mJ/cm^2 and the substrate temperature is room temperature (RT). We can observe from this figure that, in the case of using 308 nm, the surface temperature for any thickness more rapidly increases with time owing to an absorption length of less than 10 nm, as compared with the case of using 532 nm. Also, the temperature rising rate for the thinner film is higher because the absorbed energy density per unit thickness is larger in the thinner film. On the contrary, in the case of using 532 nm, the heating effect depends strongly on film thickness owing to multireflection as expected from Fig. 3. The temperature of the 60-nm-thick film is the highest among the three films of different thicknesses because the a_m is largest. Furthermore, it is noticeable that the surface temperature reaches the melting point within a time comparable to that in the case of using 308 nm although α for 532 nm is much smaller than that for 308 nm. As mentioned before, the α for 532 nm strongly depends on temperature or increases from ~10^4 to ~2.1×10^5 1/cm with temperature from RT to 1600 K, respectively. Thus, the temperature rising rate increases owing to this positive temperature-dependent absorption. However, this reason is true not only for 60 nm but also for any other thickness. The other reasons can be considered as follows: One is difference in power reflectance whose larger value means that the transmitted beam energy into the Si film is more reduced. For example, the power reflectance without multireflection for 308 nm is 0.587 which is larger than 0.374 for 532 nm at RT. Furthermore, taking multireflection into account for 532 nm, the R_m for 60 nm is much reduced to 0.125. This small R_m leads to a maximum a_m at about 60 nm as shown in Fig. 3. Second, although the optical absorption region for 308 nm is limited in the shallow surface region, that for 532 nm is in all over the film owing to its small α so that the film can be heated effectively as a whole. This whole heating effect can be observed as a higher rising rate of the 60-nm-thick film for 532 nm after 20 ns than any one for 308 nm. From this calculation result, we can conclude that the multireflection should be taken into account in an

annealing process using a green laser.

Figure 5(a) shows the theoretical calculation results of the relationships between the ac component ratios P_c of $P_n(x)$ and the grating period Λ for 30- to 80-nm-thick crystal solid Si films at $\theta_i = 0$ and $h = 1$ nm. For $\theta_i = 0$, ϕ_p is either 0 or ±180° at which P_c is positive or negative, respectively, and $P_s = 0$. As you can see from this figure, the peak of P_c for each thickness appears around $\Lambda = 530$ nm which corresponds to Rayleigh's diffraction condition of $\Lambda \approx \lambda/[n_a(1\pm\sin\theta_i)]$.[18-20] Also, it is found that when the thickness is changed from 30 to 40 nm or 60 to 70 nm, the peak polarity also changes from positive to negative or negative to positive, respectively. This polarity transition with respect to thickness can be estimated more precisely as shown in Fig. 5(b) for 39, 40, 60 and 61 nm thicknesses. It can be noted from this figure that the lower and upper critical thicknesses are about 40 and 60 nm, respectively, for P_c-Λ characteristics and that the change from 39 to 40 nm is much larger than that from 60 to 61 nm. From this result, it can be expected theoretically that periodic E-D or periodic surface structure is produced on the surface of the film with 40 nm $\leq d \leq$ 60 nm because of their negative peaks or $\phi_p = \pm 180°$ in P_c-Λ characteristics, otherwise it is hardly produced. Therefore, it can be concluded that the multireflection effect in the Si film is a crucial factor for the formation of the periodic surface structure for 532 nm. By increasing the film temperature, the P_c-Λ characteristics are shifted slightly to those of the thicker films at RT owing to the temperature dependence of the refractive index of Si. Because the temperature dependence of P_c is not as strong as the thickness dependence, we will not discuss P_c with respect to temperature further.

Figure 6 shows the theoretical calculation results of the relationships between P_c and Λ as a function of the thickness of those shown in the molten Si film at the melting point of Si. The other calculation conditions are the same as Fig. 5. Even though the film is almost opaque for 532 nm, we used N of eq. (2) with n = 2.35-i4.8. As you can note from this figure, each calculation result for 30 to 80 nm overlaps almost on the same curve. This is because the absorption length of the molten Si for 532 nm is about 10 nm and is much smaller than the film thicknesses. That is, the multireflection effect in the molten Si film thicker than 30 nm is almost ignored. Moreover, because

the peaks at about Λ = 530 nm are negative and sharp, the periodic E-D is produced steadily. The surface roughness of molten Si decreases owing to the low viscosity of Si, and the damping time is estimated roughly to be 13 ns.[21, 28] Since this estimation time is much larger than half of the pulse width of 6-7 ns, it is inferred that the liquid phase of the Si film largely contributes to the generation of the periodic E-D or formation of the surface structure. However, this calculation result for the molten Si film never suggests that film thickness is not an important parameter for the melting-crystallization process using a green laser. Melting-crystallization is never performed without melting a solid Si film. If the phase ϕ_p in $P_n(x)$ on the molten film is out of that on the solid film, the periodic T-D is not formed stably during the process from the solid phase to the liquid phase. This is because the temperature distribution depends on the heating record from the solid state to the liquid state of the film. Therefore, film thickness must be controlled as well as possible so that the phase of the periodic E-D generated on the solid Si film can be matched with the one on the molten film.

Finally, we checked experimentally the theoretical calculation of the multireflection effect on periodic structure formation. Figure 7 shows the film thickness dependence of the periodic structure area ratio to the observed irradiation area of the crystallized Si film. Also, in the inset, a scanning electron microscope (SEM) image of the 60-nm-thick melting-crystallized Si film is shown, where the film was Secco's-etched to delineate the grain boundaries. From the SEM image, it can be note that the periodic grain boundaries are formed owing to the periodic E-D and are aligned parallel to one another with a space period of being near the laser wavelength λ. In the experiment, since the maximum rising temperature in the Si film strongly depends on the film thickness d owing to the multireflection effect as shown in Fig. 3, we changed F from 110 to 170 mJ/cm^2 in order to obtain the suitable annealing condition for each thickness. The ratio of 100% means that the whole observed area (50 × 50 μm^2) of the crystallized Si film has the periodic surface structure. From this figure, we can see clearly that the periodic structure area ratios are almost 100% for the thicknesses from 50 to 65 nm while they are almost zero for the films thinner than 50 nm or thicker than 70 nm for any laser energy density. Compared with the theoretical film thickness suitable for periodic

surface structure formation from 40 to 60 nm as shown in Fig. 4, the experimental data are shifted toward larger thicknesses as a whole. One of the reasons for this difference can be that the effective refractive index N does not contain the surface roughness information as mentioned in §2. Furthermore, we can explain the difference qualitatively as follows: In order to produce the periodic structure in the film, more than one irradiation pulse is required. The first pulse increases the surface roughness of the film and the following pulse irradiation produces the periodic structure from the increased surface roughness. The surface of the first irradiated film became rough apparently although the surface of the as-deposited film was almost smooth. This suggests that the experimental film thickness suitable for the periodic structure formation may be different from the theoretical one. As an example, we will consider the case that the thickness of the as-deposited film d is 63 nm. After the first irradiation, the film thickness of some partial region decreases to less than 60 nm which is a suitable condition for periodic structure formation. Then, it is possible to produce the periodic structure in the 63-nm-thick film. However, if the thickness of the as-deposited film is much larger than 60 nm, it is probably impossible to produce the periodic structure because regions thinner than 60 nm might be few. On the other hand, the theoretical minimum critical thickness is 40 nm as shown in Fig. 5, but the experimental one is almost equal to 50 nm. It seems that this difference between the theoretical and experimental values is relatively large, compared with that for maximum critical thickness of about 60 nm. It can be explained not only by the above model of surface roughness but also by the following reason. From the theoretical calculation result shown in Fig. 5(b), it can be noted that the peak values of P_c in a polarity change from 39 to 40 nm are much larger than those from 60 to 61 nm. That is, the transition in P_c accompanied by a polarity change from 39 to 40 nm is much more abrupt than that from 60 to 61 nm. Therefore, we speculate that the periodic structure in the 40- to 50-nm-thick film may be more hardly and critically formed than that in the 60- to 70-nm-thick film probably because the sharp transition in P_c with respect to thickness brings some disturbance in the generation of periodic E-D.

5. Conclusions

We investigated the multireflection effect on the generation of the periodic E-D produced by irradiation with the linearly polarized Nd:YAG laser beam with 532 nm in the Si film deposited on the transparent glass substrate, as well as on the heating rate in the film, as compared with the excimer laser beam. From the theoretical calculation result, it was found that the generation of the periodic E-D as well as the heating rate strongly depended on film thickness, which means that the multireflection effect strongly influences the E-D and temperature in the film. The thickness to be most effective for heating rate was about 60 nm at which the power reflectance was lowest and the absorptivity per unit thickness was highest in the thickness region less than 100 nm. Thus, we should take multireflection effect into account carefully when we use a green laser beam in an annealing process. Although, in general, it seems that a green laser is not suitable to melt an Si film owing to its small absorption coefficient, this calculation result suggests that the application of the multireflection effect may be a solution to this issue.

Furthermore, we tried to verify the above calculation results by carrying out an experiment, in which we checked whether the periodic structure was formed on the surface of the melting-crystallized Si films of several thicknesses from 46 to 78 nm. As a result, it was found that the thickness range for producing the periodic E-D was from 50 to 70 nm which were larger than the theoretical values of 40 to 60 nm. It was speculated that the reason for this difference was the surface roughness or variation in thickness of the whole Si film irradiated by the first pulse. We should carry out further investigations in order to clarify this.

1) T. Sameshima, S. Usui, and M. Sekiya: IEEE Electron Device Lett. **7** (1986) 276.

2) K. Sera, F. Okumura, H. Uchida, S. Itoh, S. Kaneko, and K. Hotta: IEEE Electron Device Lett. **36** (1989) 2868.

3) H. J. Kim and J. S. Im: Appl. Phys. Lett. **68** (1996) 1513.

4) M. Ozawa, C.-H. Oh, and M. Matsumura: Jpn. J. Appl. Phys. **38** (1999) 5700.

5) A. Hara and N. Sasaki: Jpn. J. Appl. Phys. **39** (2000) L1.

6) D.-H. Choi, K. Shimizu, O. Sugiura, and M. Matsumura: Jpn. J. Appl. Phys. **31** (1992) 4545.

7) K. Shimizu, O. Sugiura, and M. Matsumura: IEEE Electron Device Lett. **40** (1993) 112.

8) R. Ishihara and P. Ch. van der Wilt: Jpn. J. Appl. Phys. **37** (1998) L15.

9) L. Mariucci, R. Carluccio, A. Pecora, V. Foglietti, G. Fortunato, and D. D. Sala: Jpn. J. Appl. Phys. **38** (1999) L907.

10) B. Rezek, C. E. Nebel, and M. Stutzmann: Jpn. J. Appl. Phys. **38** (1999) L1083.

11) C.-H. Oh, M. Ozawa, and M. Matsumura: Jpn. J. Appl. Phys. **37** (1998) L492.

12) Y.Taniguchi, M. Matsumura, M. Jyumonji, H. Ogawa, and M. Hiramatsu: J. Electrochem. Soc. **153** (2006) G67.

13) S. Horita, Y. Nakata, and A. Shimoyama: Appl. Phys. Lett. **78** (2001) 2250.

14) Y. Nakata, H. Kaki, and S. Horita: Mater. Res. Soc. Symp. Proc. **715** (2002) 199.

15) C. T. Walters: Appl. Phys. Lett. **25** (1974) 696.

16) H. J. Leamy, G. A. Rozgonyi, T. T. Sheng, and G. K. Celler: Appl. Phys. Lett. **32** (1978) 535.

17) M. Oron and G. Sϕrensen: Appl. Phys. Lett. **35** (1979) 782.

18) A. E. Siegman and P. M. Fauchet: IEEE J. Quantum Electron. **22** (1986) 1384.

19) J. F. Young, J. E. Sipe, J. S. Preston, and H. M. van Driel: Appl. Phys. Lett. **41** (1982) 261.

20) J. F. Young, J. S. Preston, H. M. van Driel, and J. E. Sipe: Phys. Rev. B **27** (1983) 1155.

21) D. K. Fork, G. B. Anderson, J. B. Boyce, R. I. Johnson, and P. Mei: Appl. Phys. Lett. **68** (1996) 2138.

22) H. Kaki and S. Horita: J. Appl. Phys. **97** (2005) 014904.

23) D. F. Edwards: in *Handbook of Optical Constants of Solid*, ed. E. D. Palik (Academic, San Diego, 1985) p. 547.

24) Y. F. Tang, S. R. P. Silva, and M. J. Rose: Appl. Phys. Lett. **78** (2001) 186.

25) T. Kudo, K. Yamazaki, and T. Akashi: Proc. 11th Int. Display Workshops, Niigata, *2004*, p. 619.

26) C.-L. Fan, T.-H. Yang, and C.-I. Lin: Jpn. J. Appl. Phys. **45** (2006) L973.

27) S. Horita, K. Nishioka, and H. Kaki: Proc. 12th Int. Display Workshops, Takamatsu, 2005, p. 1191.

28) R. F. Wood and G. A. Geist: Phys. Rev. B **34** (1986) 2606.

29) G. E. Jellison, Jr.: in *Semiconductors and Semimetals*, ed. R. F. Wood, C. W. White, and R. T. Young (Academic, Orlando, 1984) Vol. 23, p. 95.

30) Z. Guosheng, P. M. Fauchet, and A. E. Siegman: Phys. Rev. B **26** (1982) 5366.

31) S. Horita, H. Kaki, and K. Nishioka: submitted to J. Appl. Phys.

32) Y. Nakata, H. Kaki, and S. Horita: Jpn. J. Appl. Phys. **43** (2004) 2630.

Figure Captions

Fig. 1 Schematic model of the layered structure sample consisting of an Si film deposited on a SiO_2 substrate for calculation of heating rate on the surface of the Si film. In the Si film, multireflection of 532 nm laser beam occurs.

Fig. 2 Schematic models of (a) the layered structure sample with the sinusoidally corrugated surface of the Si film and (b) the optically equivalent bulk-like sample for calculation of periodic E-D. The primary incident beam is diffracted on the sinusoidally corrugated surface and n indicates the order of the diffracted beam.

Fig. 3 Theoretical calculation results of the dependences of the absorptivity A_m and the absorptivity per unit thickness a_m on the thickness of the solid film d for 532 nm. $A_m \equiv 1\text{-}R_m\text{-}T_m$ and $a_m \equiv A_m/d$, where the R_m and T_m are the overall power reflectance and transmittance, respectively.

Fig. 4 Time dependences of surface temperature of an irradiated solid Si film on a SiO_2 substrate for 308 nm (excimer) and 532 nm (Nd:YAG). The film thicknesses are 40, 60 and 80 nm. For both wavelengths, F is 250 mJ/cm^2 and the substrate temperature is room temperature. In the 60-nm-thick film for 532 nm, a more constructive interference occurs through multireflection.

Fig. 5 Theoretical calculation results of the relationships between the ac component ratio P_c of $P_n(x)$ and the grating period Λ (a) for 30-, 40-, 50-, 60-, 70-, and 80-nm-thick, and (b)for 39-, 40-, 60-, and 61-nm-thick crystal solid Si films at $\theta_1 = 0$, h = 1 nm and room temperature. From (b), it is found that negative peaks of P_c disappear at 39 and 61 nm and that the lower and upper critical thickness for the generation of periodic E-D are approximately 40 and 60 nm, respectively.

Fig. 6 Theoretical calculation results of the relationships between P_c and Λ as a function of the thickness of the molten Si film at the melting point of Si. The other calculation conditions are the

same as those shown in Fig. 5.

Fig. 7 Film thickness dependence of the periodic structure area ratio to the observed irradiation area 50 × 50 μm^2 of the crystallized Si film. The inset shows an SEM image of the 60-nm-thick melting-crystallized Si film, where the film was Secco's-etched to delineate the grain boundaries.

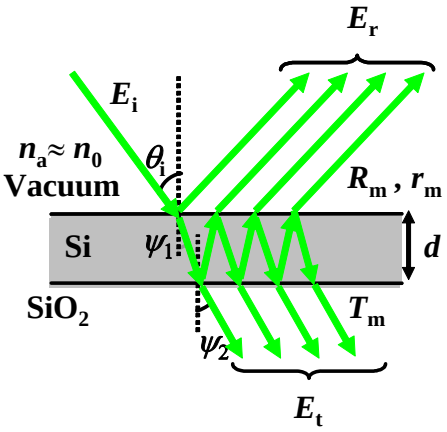

Fig. 1

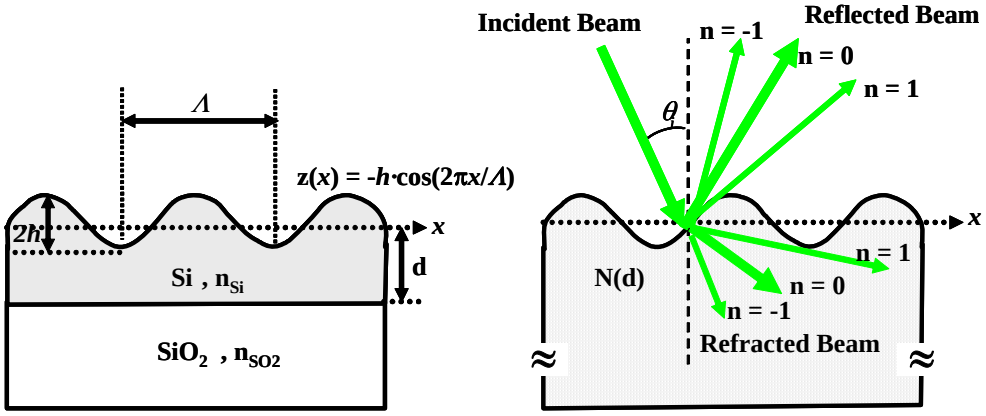

(a) Thin Film Sample **(b) Equivalent Bulk Model**

Fig. 2

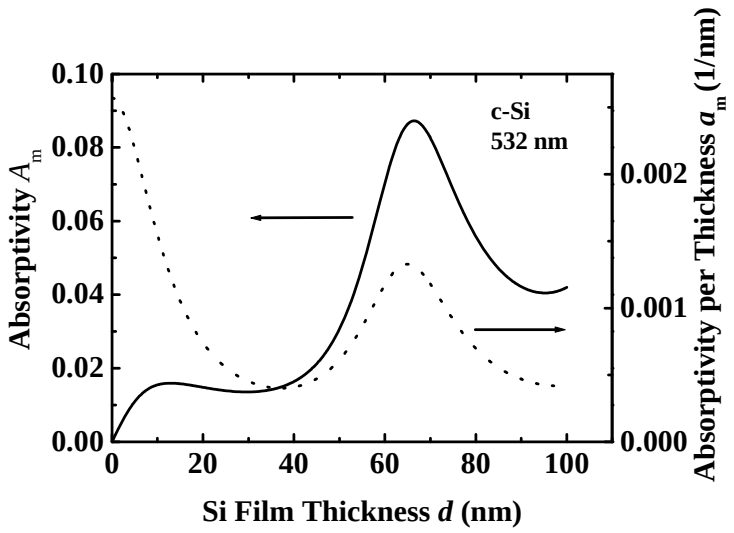

Fig. 3

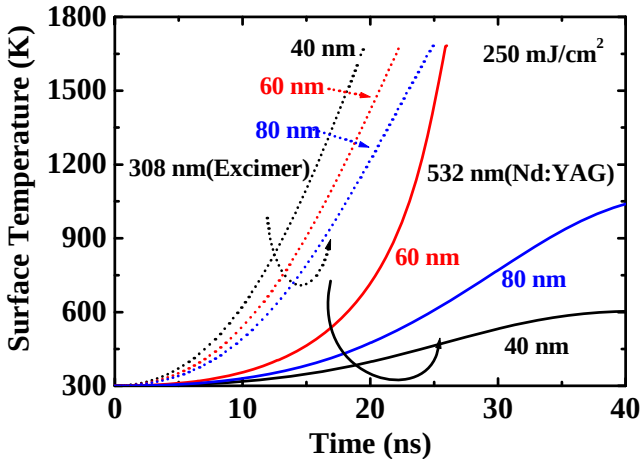

Fig. 4

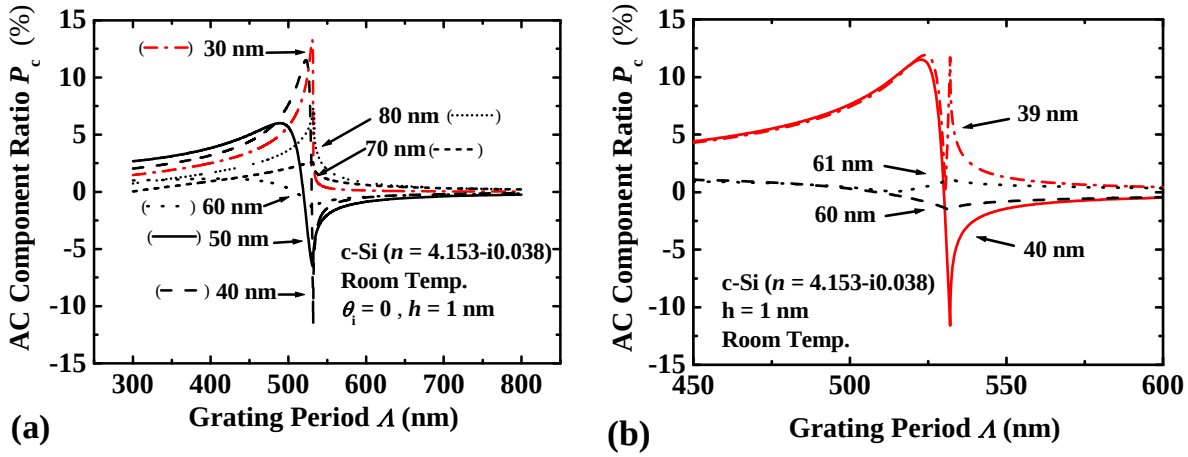

Fig. 5

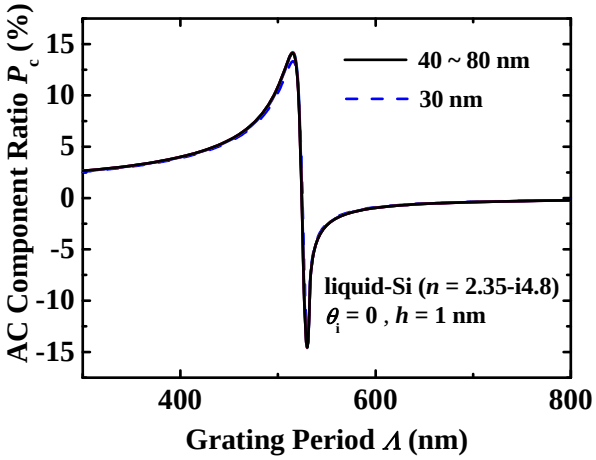

Fig. 6

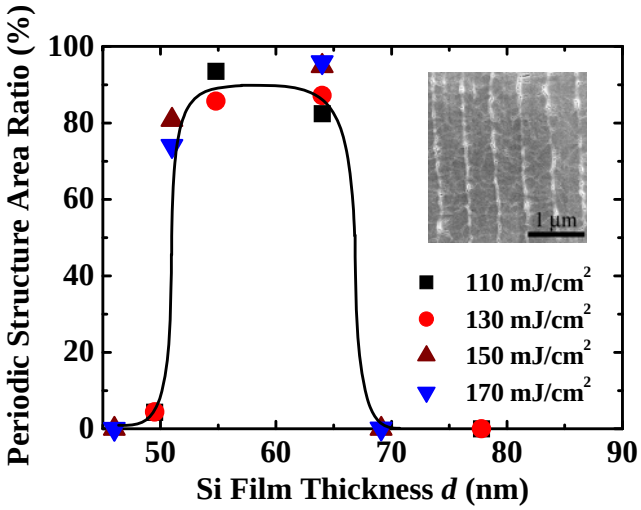
Periodic Structure Area Ratio (%)
100
80
60
40
20
0
50
60
70
80
90
Si Film Thickness d (nm)
1 μm
110 mJ/cm2
130 mJ/cm2
150 mJ/cm2
170 mJ/cm2

Fig. 7